2026 IEEE/SICE International Symposium on System Integration (SII)
January 11-14, 2026. Cancún, México

Trajectory Generation for Tip-Over Prevention and Collision Avoidance of Automatic Excavators

Kenshiro Yamashita[1] and Ryo Kikuuwe[1]

***Abstract*— This paper proposes a method for generating end-effector trajectories for automatic excavators to prevent tipping over and avoid collisions with obstacles. The criterion for determining whether the excavator is at risk of tipping over is derived using the Zero-Moment Point (ZMP), which represents the center of reaction forces. A simplified model of the excavator is used in this derivation to avoid complexity. Additionally, the end-effector trajectories are automatically generated by using an algorithm based on the penalty function method, which incorporates constraints to prevent both tipping over and collisions with nearby obstacles. The automated excavator followed the generated trajectories in a simulator, and it was confirmed that tipping over was prevented and collisions with obstacles were avoided.**

I. INTRODUCTION

The automation of hydraulic excavators is a crucial issue for improving efficiency and safety at construction sites. To achieve this, trajectory generation technology is needed to determine end-effector trajectories that do not result in tipping over or collisions and that complete the tasks as quickly as possible. Tsuziki et al. [1] generated a hierarchical model of backfilling trajectories using an automated excavator based on soil geometry and trajectory data from a skilled operator, and attempted to generate an optimal trajectory that is efficient and mimics the trajectory of a skilled operator. Son et al. [2] implemented automation by imitating the trajectories of skilled operators in a way that prevents excessive forces on the excavator. Zhang et al. [3] used sequential quadratic programming to find optimal time and jerk trajectories during operation, allowing the hydraulic excavator to perform stable and efficient movements.

This paper proposes a method for generating end-effector trajectories focused on preventing tipping over and avoiding collisions with obstacles for automated excavators. The criterion for determining whether the excavator is at risk of tipping over is derived from the ZMP of a simplified model of the excavator. Furthermore, the end-effector trajectories are automatically generated using an algorithm based on the penalty function method. The automated excavator follows the generated trajectories in simulations, and it is confirmed that tipping over is successfully prevented and obstacles are avoided.

*This work was supported by Kobelco Construction Machinery Co., Ltd.
[1]Machinery Dynamics Laboratory, Hiroshima University, 1-4-1 Kagamiyama, Higashi-Hiroshima, Hiroshima 739-8527, Japan. (e-mail:m240384@hiroshima-u.ac.jp; kikuuwe@ieee.org)

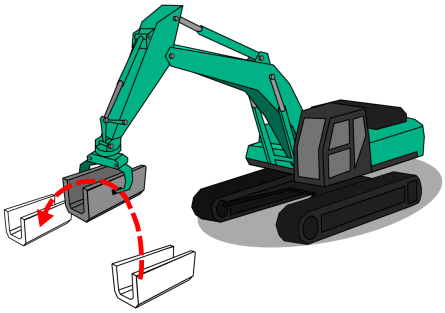

Fig. 1: Excavator for handling precast concrete blocks.

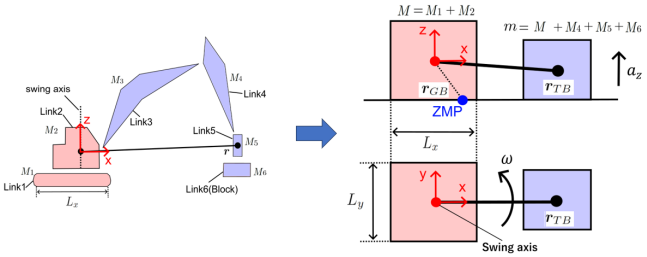

Fig. 2: Simple model.

II. TIPPING OVER OF EXCAVATORS

A. Simple Model of Excavators

The excavator consists of a lower body, an upper body, a boom, an arm, and a grapple. This excavator is used for handling precast concrete blocks, as shown in Fig. 1. In this paper, the excavator is divided into two parts: non-moving and moving parts. The non-moving part includes the lower and upper body, while the moving part includes the boom, arm, grapple, and block. Both parts, as well as the actuators connecting them, are treated as rigid bodies. The masses of the non-moving and moving parts are denoted by M and m, respectively. A simplified model of the excavator is shown in Fig. 2. Here, $\boldsymbol{r}_{TB} \in \mathbb{R}^3$ represents the vector from the non-moving part to the moving part, and $\boldsymbol{r}_{GB} \in \mathbb{R}^3$ represents the vector from the non-moving part to the ZMP. The lengths of the non-moving part in the x and y directions are denoted by L_x and L_y, respectively.

B. ZMP of Excavators

To evaluate the stability of an excavator, we consider ZMP, which is the point on the ground where the horizontal component of the moment generated by external forces becomes zero. Let $\boldsymbol{f} \in \mathbb{R}^3$ be the external force acting on

the system and $\boldsymbol{\tau} \in \mathbb{R}^3$ the total moment about a reference point. In general, the vector $\boldsymbol{r} \in \mathbb{R}^3$ satisfying

$$\boldsymbol{\tau} = \boldsymbol{r} \times \boldsymbol{f} \tag{1}$$

is obtained as

$$\boldsymbol{r} = \frac{\boldsymbol{f} \times \boldsymbol{\tau}}{\|\boldsymbol{f}\|^2} + \kappa \boldsymbol{f} \tag{2}$$

where $\kappa \in \mathbb{R}$. Applying the above general relation specifically to the excavator model, the ZMP $\boldsymbol{r}_{GB}$ is expressed as follows:

$$\begin{aligned}\boldsymbol{r}_{GB} = &\frac{(\boldsymbol{f}_{TB} - M\boldsymbol{g}) \times (\boldsymbol{r}_{TB} \times \boldsymbol{f}_{TB} + \boldsymbol{\tau}_{TB})}{\|\boldsymbol{f}_{TB} - M\boldsymbol{g}\|^2} \\ &+\kappa(\boldsymbol{f}_{TB} - M\boldsymbol{g})\end{aligned} \tag{3}$$

Here, the force and torque exerted by the actuator on the moving part are denoted by $\boldsymbol{f}_{TB} \in \mathbb{R}^3$ and $\boldsymbol{\tau}_{TB} \in \mathbb{R}^3$, respectively. κ is an arbitrary real number. Let the z-axis be directed vertically upward. The gravitational acceleration vector is $\boldsymbol{g} = [0, 0, -g]^T$. This paper also defines $\tilde{\boldsymbol{f}}_{TB} \triangleq \boldsymbol{f}_{TB} + m\boldsymbol{g}$, which indicates that when the non-moving part is at rest, $\tilde{\boldsymbol{f}}_{TB} = 0$. Equation (3) shows that the ZMP is not fixed at a single point due to an arbitrary real number κ, but the ZMP must be positioned on the ground. Let $H > 0$ be the height of the center of mass of the non-moving part from the ground. By solving for κ so that the z-component of $\boldsymbol{r}_{GB}$ equals $-H$, $\boldsymbol{r}_{GB}$ is expressed as follows:

$$\begin{aligned}\boldsymbol{r}_{GB} = &-\begin{bmatrix} 0 \\ 0 \\ H \end{bmatrix} + \frac{mg + \tilde{f}_{TB,z}}{(M+m)g + \tilde{f}_{TB,z}} \begin{bmatrix} r_{TB,x} \\ r_{TB,y} \\ 0 \end{bmatrix} \\ &-\frac{H + r_{TB,z}}{(M+m)g + \tilde{f}_{TB,z}} \begin{bmatrix} \tilde{f}_{TB,x} \\ \tilde{f}_{TB,y} \\ 0 \end{bmatrix}\end{aligned} \tag{4}$$

In (4), the torque $\boldsymbol{\tau}_{TB}$ acting on the moving part is neglected, and $\tilde{\boldsymbol{f}}_{TB}$ is parallel to $\boldsymbol{r}_{TB}$. The force $\tilde{\boldsymbol{f}}_{TB}$, which is the force exerted by the actuator on the moving part, is expressed as follows:

$$\begin{aligned}\tilde{\boldsymbol{f}}_{TB} = &\, m \begin{bmatrix} 0 \\ 0 \\ a_z \end{bmatrix} - m\omega^2 \begin{bmatrix} r_{TB,x} \\ r_{TB,y} \\ r_{TB,z} \end{bmatrix} \\ &+ \frac{ma_r}{\sqrt{r_{TB,x}^2 + r_{TB,y}^2}} \begin{bmatrix} r_{TB,x} \\ r_{TB,y} \\ 0 \end{bmatrix}\end{aligned} \tag{5}$$

Here, $a_r \in \mathbb{R}$ represents the radial acceleration.

C. Tipping-over Limit

The critical vertical acceleration at which the excavator tips over is derived as a tipping-over limit during lifting operations. When lifting a block in the vertical direction, the force acting on the moving part is assumed to be only in the z-direction. In this case, $\tilde{\boldsymbol{f}}_{TB}$ is expressed as follows:

$$\tilde{\boldsymbol{f}}_{TB} = m[0, 0, a_z]^T \tag{6}$$

Tipping over occurs when the ZMP of the excavator is located on the edge of the support polygon ($r_{GB,x} = L_x/2$ and $r_{GB,y} = L_y/2$). The critical vertical acceleration at which tipping over occurs is derived to establish the tipping-over limit for lifting and lowering operations. Substituting $r_{GB,x} = L_x/2$ and $r_{GB,y} = L_y/2$ into (6) and then solving for a_z in (4), the acceleration of tipping-over limit a_{cz} is obtained as follows:

$$a_{cz,*} = \max\left(\frac{-g(L_*/2(m+M) - mr_{TB,*})}{m(L/2 - r_{TB,*})}, 0\right) \tag{7}$$

Here, $*$ represents either x or y. The acceleration of tipping-over limit that causes tipping over in the x-axis direction ($a_{cz,x}$) and the one in the y-axis direction ($a_{cz,y}$) are obtained by substituting x and y for $*$ in (7).

In addition, the critical angular velocity at which tipping over occurs is derived to establish the tipping-over limit for swinging motion. By substituting (5) into (4) and solving for ω^2, we can express it as follows:

$$\begin{aligned}\omega^2 &= \mathrm{g}(r_{GB,*}) \\ &= \Big(g\left(r_{GB,*}(1 + M/m)/2 - r_{TB,x}\right) \\ &\quad + a_z\left(r_{GB,*}/2 - r_{TB,x}\right) \\ &\quad + a_r H r_{TB,x}/\sqrt{r_{TB,x}^2 + r_{TB,y}^2}\Big) \\ &\quad \Big/ \left(r_{TB,x} r_{GB,z} - \left(r_{GB,*}/2 - r_{TB,x}\right) r_{TB,z}\right)\end{aligned} \tag{8}$$

Here, $a_z \in \mathbb{R}$ represents the vertical acceleration. Substituting $r_{GB,x} = L_x/2$ and $r_{GB,y} = L_y/2$ into (8), the angular velocity of tipping-over limit (Ω_c) is obtained as follows:

$$\Omega_{c,*} = \sqrt{\max\left(\mathrm{g}(L_*/2), 0\right)} \tag{9}$$

The angular velocity of tipping-over limit that causes tipping over in the x-axis direction ($\Omega_{c,x}$) and in the y-axis direction ($\Omega_{c,y}$) are derived by substituting x and y for $*$ in (9).

If any of $a_{cz,x}$, $a_{cz,y}$, $\Omega_{c,x}$, or $\Omega_{c,y}$ equals zero, it indicates a risk of tipping over, regardless of the operations being performed by the excavator.

III. Trajectory Generation

A. Time-series Data of Trajectory

Here, we consider designing an end-effector trajectory for an excavator in cylindrical coordinates over a given duration. With a sampling interval of T, the trajectory over the duration TN is represented by a $3N$-dimensional vector $\boldsymbol{P} \in \mathbb{R}^{3N}$. This vector consists of three N-dimensional time series corresponding to the cylindrical coordinates $\boldsymbol{\theta} \in \mathbb{R}^N$, $\boldsymbol{r}_r \in \mathbb{R}^N$, and $\boldsymbol{r}_z \in \mathbb{R}^N$, which represent the angular position, radial distance, and vertical height of the arm end, respectively.The trajectory vector $\boldsymbol{P}$, as well as the corresponding velocity $\boldsymbol{V} \in \mathbb{R}^{3N}$ and acceleration $\boldsymbol{A} \in \mathbb{R}^{3N}$, are defined as follows:

$$\boldsymbol{P} \triangleq \mathrm{vec}([\boldsymbol{\theta}, \boldsymbol{r}_z, \boldsymbol{r}_r]^T) \in \mathbb{R}^{3N} \tag{10}$$

$$\boldsymbol{V} \triangleq \mathrm{vec}([\boldsymbol{\omega}, \boldsymbol{v}_z, \boldsymbol{v}_r]^T) \in \mathbb{R}^{3N} \tag{11}$$

$$\boldsymbol{A} \triangleq \mathrm{vec}([\boldsymbol{\alpha}, \boldsymbol{a}_z, \boldsymbol{a}_r]^T) \in \mathbb{R}^{3N} \tag{12}$$

where $\boldsymbol{\omega}, \boldsymbol{\alpha} \in \mathbb{R}^N$ are the angular velocity and angular acceleration, and $\boldsymbol{v}_r, \boldsymbol{a}_r, \boldsymbol{v}_z, \boldsymbol{a}_z \in \mathbb{R}^N$ represent the velocities and accelerations in the radial and vertical directions,

respectively. The function $\mathrm{vec}(\boldsymbol{X})$ indicates the operation of vectorizing a matrix $\boldsymbol{X}$ by stacking its columns into a single column vector. Therefore, the function vec is applied to vectors $\boldsymbol{x}, \boldsymbol{y}, \boldsymbol{z} \in \mathbb{R}^N$ as follows:

$$\mathrm{vec}([\boldsymbol{x}, \boldsymbol{y}, \boldsymbol{z}]^T) \triangleq [x_{(1)}, y_{(1)}, z_{(1)}, \cdots, x_{(N)}, y_{(N)}, z_{(N)}]^T \tag{13}$$

Assuming a constant sampling interval T, the velocity and position trajectories can be obtained by integrating the acceleration data over time. Therefore, once the acceleration $\boldsymbol{A}$ is determined, the velocity $\boldsymbol{V}$ and position $\boldsymbol{P}$ can also be computed using the following relations:

$$\boldsymbol{V} \triangleq \boldsymbol{D}_{3N}\boldsymbol{A}, \tag{14}$$

$$\boldsymbol{P} \triangleq \boldsymbol{D}_{3N}\boldsymbol{V}, \tag{15}$$

where $\boldsymbol{D}_{3N} \in \mathbb{R}^{3N\times 3N}$ is a discrete integration matrix defined as follows:

$$\boldsymbol{D} \triangleq \begin{bmatrix} 0 & \cdots & \cdots & 0 \\ T & \ddots & \ddots & \vdots \\ \vdots & \ddots & \ddots & \vdots \\ T & \cdots & T & 0 \end{bmatrix} \in \mathbb{R}^{N\times N} \tag{16}$$

$$\boldsymbol{I} \triangleq \mathrm{diag}(1,1,1) \in \mathbb{R}^{3\times 3} \tag{17}$$

$$\boldsymbol{D}_{3N} \triangleq \boldsymbol{D} \otimes \boldsymbol{I} \in \mathbb{R}^{3N\times 3N} \tag{18}$$

In (18), $\boldsymbol{D} \otimes \boldsymbol{I}$ denotes the Kronecker product.

B. Trajectory Generation by Using Penalty Function

An automated hydraulic excavator must perform tasks as quickly and efficiently as possible while avoiding tipping over and collisions with obstacles. To achieve such operations, generating an appropriate end-effector trajectory in advance is necessary. The objective function and constraints for end-effector trajectory generation are presented as follows:

$$\underset{\boldsymbol{A},t_F}{\text{minimize}} \quad w_a J_A + w_{tf} J_{tf} \tag{19a}$$

$$\text{s.t.} \quad A_k = 0 \qquad \forall k \geq k_F \tag{19b}$$

$$A_k \leq A_{\max,k} \qquad \forall k \geq 0 \tag{19c}$$

$$A_k \geq A_{\min,k} \qquad \forall k \geq 0 \tag{19d}$$

$$V_k = 0 \qquad \forall k \geq k_F \tag{19e}$$

$$V_k \leq V_{\max,k} \qquad \forall k \geq 0 \tag{19f}$$

$$V_k \geq V_{\min,k} \qquad \forall k \geq 0 \tag{19g}$$

$$P_k = P_{d,k} \qquad \forall k \geq k_F \tag{19h}$$

$$\boldsymbol{r}_{TB,k} \notin \boldsymbol{R}_{\text{obs}} \quad \forall k \geq 0 \tag{19i}$$

$$r_{z,k} \geq h_l \qquad k = k_F/2 \tag{19j}$$

$$\sqrt{r_{TB,x,k}^2 + r_{TB,y,k}^2} \geq r_{\text{lim}} \quad \forall k \geq 0 \tag{19k}$$

Here, $w_* \in \mathbb{R}$ are the weight parameters. t_F represents the terminal time of tasks. $\boldsymbol{R}_{\text{obs}}$ denotes the region where obstacles are set, and r_{lim} is a minimum radius that the end-effector cannot enter. h_l is the height set to prevent the end-effector from contacting the ground. The terms J_A and J_{tf} are defined as follows:

$$J_A \triangleq \frac{1}{2}\|\boldsymbol{A}\|^2 \tag{20}$$

$$J_{tf} \triangleq t_F \tag{21}$$

$\boldsymbol{P}_d \in \mathbb{R}^{3N}$ represents the target position of the trajectory and is defined as follows:

$$\boldsymbol{P}_d \triangleq \mathrm{vec}([\boldsymbol{\theta}_d, \boldsymbol{0}_N, \boldsymbol{r}_{r,d}]) \in \mathbb{R}^{3N} \tag{22}$$

The constraints from (19b) to (19k) include conditions to set $\boldsymbol{A}$ and $\boldsymbol{V}$ to zero after t_F, ensure that $\boldsymbol{P}$ reaches the target value, and prevent the excavator from exceeding its maximum specifications. They also include conditions to avoid tipping over and collisions, and ensure that the end-effector does not drag on the ground. While satisfying these constraints, $\boldsymbol{A}$ and t_F are found that minimize $w_a J_A + w_{tf} J_{tf}$. Since (19a) is hard to solve directly, the constraints, including nonlinear ones, are incorporated as penalty terms, which allows flexible handling of various constraint types, and a new minimization problem is formulated. The resulting new minimization problem is as follows:

$$\underset{\boldsymbol{A},t_F}{\text{minimize}} \quad J_p \tag{23}$$

Here,

$$J_p \triangleq w_a J_A + w_{tf} J_{tf} + w_{at} J_{AT} + w_{vt} J_{VT} + w_{pt} J_{PT} \tag{24a}$$

$$J_{AT} \triangleq \|\boldsymbol{A}_P\| \tag{24b}$$

$$J_{VT} \triangleq \|\boldsymbol{V}_P\| \tag{24c}$$

$$J_{PT} \triangleq \|\boldsymbol{P}_P\| \tag{24d}$$

$$\boldsymbol{A}_P \triangleq \max(\boldsymbol{A} - \boldsymbol{A}_{\max}, \boldsymbol{0}) + \min(\boldsymbol{A} - \boldsymbol{A}_{\min}, \boldsymbol{0}) \tag{24e}$$

$$\boldsymbol{V}_P \triangleq \max(\boldsymbol{V} - \boldsymbol{V}_{\max}, \boldsymbol{0}) + \min(\boldsymbol{V} - \boldsymbol{V}_{\min}, \boldsymbol{0}) \tag{24f}$$

$$\boldsymbol{P}_P \triangleq \max(\boldsymbol{P} - \boldsymbol{P}_{\max}, \boldsymbol{0}) + \min(\boldsymbol{P} - \boldsymbol{P}_{\min}, \boldsymbol{0}) \tag{24g}$$

$$\boldsymbol{A}_{\max} \triangleq \mathrm{vec}([\boldsymbol{\alpha}_{\max}, \boldsymbol{a}_{z,\max}, \boldsymbol{a}_{r,\max}]) \in \mathbb{R}^{3N} \tag{24h}$$

$$\boldsymbol{A}_{\min} \triangleq \mathrm{vec}([\boldsymbol{\alpha}_{\min}, \boldsymbol{a}_{z,\min}, \boldsymbol{a}_{r,\min}]) \in \mathbb{R}^{3N} \tag{24i}$$

$$\boldsymbol{V}_{\max} \triangleq \mathrm{vec}([\boldsymbol{\omega}_{\max}, \boldsymbol{v}_{z,\max}, \boldsymbol{v}_{r,\max}]) \in \mathbb{R}^{3N} \tag{24j}$$

$$\boldsymbol{V}_{\min} \triangleq \mathrm{vec}([\boldsymbol{\omega}_{\min}, \boldsymbol{v}_{z,\min}, \boldsymbol{v}_{r,\min}]) \in \mathbb{R}^{3N} \tag{24k}$$

$$\boldsymbol{P}_{\max} \triangleq \mathrm{vec}([\boldsymbol{\theta}_{\max}, \boldsymbol{r}_{z,\max}, \boldsymbol{r}_{r,\max}]) \in \mathbb{R}^{3N} \tag{24l}$$

$$\boldsymbol{P}_{\min} \triangleq \mathrm{vec}([\boldsymbol{\theta}_{\min}, \boldsymbol{r}_{z,\min}, \boldsymbol{r}_{r,\min}]) \in \mathbb{R}^{3N} \tag{24m}$$

$$\boldsymbol{\alpha}_{\max} \triangleq \left[(\boldsymbol{\alpha}_{\text{sp}})_{k_F}^T, \boldsymbol{0}_{(k_F+1:N)}^T\right]^T \in \mathbb{R}^N \tag{24n}$$

$$\boldsymbol{a}_{r,\max} \triangleq \left[(\boldsymbol{a}_{r,\text{sp}})_{k_F}^T, \boldsymbol{0}_{(k_F+1:N)}^T\right]^T \in \mathbb{R}^N \tag{24o}$$

$$\boldsymbol{a}_{z,\max} \triangleq \left[(\min(\boldsymbol{a}_{z,\text{sp}}, \boldsymbol{a}_{cz}))_{k_F}^T, \boldsymbol{0}_{(k_F+1:N)}^T\right]^T \in \mathbb{R}^N \tag{24p}$$

$$\boldsymbol{\alpha}_{\min} \triangleq \left[(-\boldsymbol{\alpha}_{\text{sp}})_{k_F}^T, \boldsymbol{0}_{(k_F+1:N)}^T\right]^T \in \mathbb{R}^N \tag{24q}$$

$$\boldsymbol{a}_{r,\min} \triangleq \left[(-\boldsymbol{a}_{r,\text{sp}})_{k_F}^T, \boldsymbol{0}_{(k_F+1:N)}^T\right]^T \in \mathbb{R}^N \tag{24r}$$

$$\boldsymbol{a}_{z,\min} \triangleq \left[(-\boldsymbol{a}_{z,\text{sp}})_{k_F}^T, \boldsymbol{0}_{(k_F+1:N)}^T\right]^T \in \mathbb{R}^N \tag{24s}$$

$$\boldsymbol{\omega}_{\max} \triangleq \left[(\min(\boldsymbol{\omega}_{\text{sp}}, \boldsymbol{\Omega}_c))_{k_F}^T, \boldsymbol{0}_{(k_F+1:N)}^T\right]^T \in \mathbb{R}^N \tag{24t}$$

$$\boldsymbol{v}_{r,\max} \triangleq \left[(\boldsymbol{v}_{r,\mathrm{sp}})_{k_F}^T, \boldsymbol{0}_{(k_F+1:N)}^T\right]^T \in \mathbb{R}^N \tag{24u}$$

$$\boldsymbol{v}_{z,\max} \triangleq \left[(\boldsymbol{v}_{z,\mathrm{sp}})_{k_F}^T, \boldsymbol{0}_{(k_F+1:N)}^T\right]^T \in \mathbb{R}^N \tag{24v}$$

$$\boldsymbol{\omega}_{\min} \triangleq \left[(-\boldsymbol{\omega}_{\mathrm{sp}})_{k_F}^T, \boldsymbol{0}_{(k_F+1:N)}^T\right]^T \in \mathbb{R}^N \tag{24w}$$

$$\boldsymbol{v}_{r,\min} \triangleq \left[(-v_{r,\mathrm{sp}})_{k_F}^T, \boldsymbol{0}_{(k_F+1:N)}^T\right]^T \in \mathbb{R}^N \tag{24x}$$

$$\boldsymbol{v}_{z,\min} \triangleq \left[(-v_{z,\mathrm{sp}})_{k_F}^T, \boldsymbol{0}_{(k_F+1:N)}^T\right]^T \in \mathbb{R}^N \tag{24y}$$

$$\boldsymbol{\theta}_{\max} \triangleq \boldsymbol{\theta}_d \in \mathbb{R}^N \tag{24z}$$

$$\boldsymbol{r}_{r,\max} \triangleq \min(\boldsymbol{r}_{r,\mathrm{sp,max}}, \boldsymbol{r}_{obs}) \in \mathbb{R}^N \tag{24aa}$$

$$\boldsymbol{r}_{z,\max} \triangleq \left[(\boldsymbol{r}_{z,\mathrm{sp}})_{k_F}^T, \boldsymbol{0}_{(k_F+1:N)}^T\right]^T \in \mathbb{R}^N \tag{24ab}$$

$$\boldsymbol{\theta}_{\min} \triangleq \left[\boldsymbol{0}_{k_F}^T, (\boldsymbol{\theta}_d)_{(k_F+1:N)}^T\right]^T \in \mathbb{R}^N \tag{24ac}$$

$$\boldsymbol{r}_{r,\min} \triangleq \left[(\boldsymbol{r}_{r,\mathrm{sp,min}})_{k_F}^T, (\boldsymbol{r}_{r,d})_{(k_F+1:N)}^T\right]^T \in \mathbb{R}^N \tag{24ad}$$

$$\boldsymbol{r}_{z,\min} \triangleq \boldsymbol{r}_h \in \mathbb{R}^N \tag{24ae}$$

$$r_{obs,k} \triangleq \begin{cases} a_k & \text{if } \ \boldsymbol{r}_{TB,k} \in \boldsymbol{R}_{\mathrm{obs}} \\ & \quad \wedge\ (h_{\max} > d_{\max} \vee \mathrm{mod}(q, n_{\mathrm{ite}}) = 0) \\ 0 & \text{otherwise} \end{cases} \tag{24af}$$

$$h_{obs,k} \triangleq \begin{cases} b_k & \text{if } \ \boldsymbol{r}_{TB,k} \in \boldsymbol{R}_{\mathrm{obs}} \\ & \quad \wedge\ (h_{\max} \leq d_{\max} \vee \mathrm{mod}(q, n_{\mathrm{ite}}) = 0) \\ 0 & \text{otherwise} \end{cases} \tag{24ag}$$

$$r_{h,k} \triangleq \mathrm{lft}(k, h_l, T, t_F) \tag{24ah}$$

Here, $a_k \in \mathbb{R}$ represents the horizontal length of the manipulator that has not penetrated into the obstacle. On the other hand, $b_k \in \mathbb{R}$ represents the vertical length from the ground to the height of the obstacle. $h_{\max} \in \mathbb{R}$ and $d_{\max} \in \mathbb{R}$ indicate the maximum vertical and radial sink lengths of the initial trajectory of the end-effector as it passes inside the obstacle, and $q \in \mathbb{N}$ indicates the the number of iterations during the minimization algorithm. Using q and $n_{\mathrm{ite}} \in \mathbb{N}$ in conditions prevents avoiding obstacles in a particular direction, which avoids reaching a local solution. Additionally, the function lft is defined as follows for $k \in \mathbb{N}$ and $h_l, T, t_F \in \mathbb{R}$.

$$\mathrm{lft}(k, h_l, T, t_F) \triangleq \begin{cases} \dfrac{kTh_l}{t_F/2} & \text{if } \ k \leq \dfrac{t_F}{2T} \\ 2h_l - \dfrac{kTh_l}{t_F/2} & \text{if } \ \dfrac{t_F}{2T} < k \leq \dfrac{t_F}{T} \\ 0 & \text{otherwise} \end{cases} \tag{25}$$

Here, α_{sp}, ω_{sp}, $a_{z,\mathrm{sp}}$, $v_{z,\mathrm{sp}}$, $a_{r,\mathrm{sp}}$, and $v_{r,\mathrm{sp}}$ represent the maximum values specified for the excavator's specifications. $r_{r,\mathrm{sp,max}}$ and $r_{r,\mathrm{sp,min}}$ represent the maximum and minimum lengths of the manipulator of the excavator. In addition, θ_d and $r_{r,d}$ denote the swinging angle and manipulator length at the end of the task, respectively. Furthermore, $\boldsymbol{0}_n \in \mathbb{R}^n$ signifies the zero vector in n-dimensions, and constants written in bold, such as $\boldsymbol{\alpha}_{\mathrm{sp}}$, represent an n-dimensional vector where all elements are equal to that constant. Moreover, $\boldsymbol{a}_{cz}$ represents the limit acceleration for tipping over for the end-effector of the excavator and corresponds to the smaller of the values $a_{cz,x}$ and $a_{cz,y}$, which are derived from the time-series data of $\boldsymbol{\theta}$. The term $\boldsymbol{\Omega}_c$ denotes the limit angular velocity for tipping over and corresponds to the smaller of the values $\boldsymbol{\Omega}_{c,x}$ and $\boldsymbol{\Omega}_{c,y}$, which are also derived from the time-series data of $\boldsymbol{\theta}$.

The following algorithm finds $\boldsymbol{A}$ and t_F that minimize the objective function J_p. J_p is differentiated by $\boldsymbol{A}$ and t_F to obtain $\boldsymbol{A}$ and t_F that satisfy the conditions. $\beta_* \in \mathbb{R}$ is used as the step width in the steepest descent method. R is a constant value such that $0 < R < 1$, which gradually reduces the step width as the iteration number increases.

$$\boldsymbol{A} \coloneqq \boldsymbol{A}_0 \tag{26a}$$

$$\beta_1 \coloneqq \beta_{1,0} \tag{26b}$$

$$\text{for } \ q = 1 : Q \tag{26c}$$

$$\boldsymbol{f}_A \coloneqq \boldsymbol{A} \tag{26d}$$

$$\boldsymbol{f}_{AT} \coloneqq \frac{\partial J_{AT}}{\partial \boldsymbol{A}} = \frac{\boldsymbol{A}_P}{\|\boldsymbol{A}_P\|} \tag{26e}$$

$$\boldsymbol{f}_{VT} \coloneqq \frac{\partial J_{VT}}{\partial \boldsymbol{A}} = \boldsymbol{D}_{3N} \frac{\boldsymbol{V}_P}{\|\boldsymbol{V}_P\|} \tag{26f}$$

$$\boldsymbol{f}_{PT} \coloneqq \frac{\partial J_{PT}}{\partial \boldsymbol{A}} = \boldsymbol{D}_{3N}^2 \frac{\boldsymbol{P}_P}{\|\boldsymbol{P}_P\|} \tag{26g}$$

$$f_{ATF} \coloneqq \frac{\partial J_{AT}}{\partial t_F} = -\frac{1}{T} \sum_{k=3k_F+1}^{3k_F+3} A_{P,k} \tag{26h}$$

$$f_{VTF} \coloneqq \frac{\partial J_{VT}}{\partial t_F} = -\frac{1}{T} \sum_{k=3k_F+1}^{3k_F+3} V_{P,k} \tag{26i}$$

$$f_{PTF} \coloneqq \frac{\partial J_{PT}}{\partial t_F} = -\frac{1}{T} \sum_{k=3k_F+1}^{3k_F+3} P_{P,k} \tag{26j}$$

$$\boldsymbol{A} \coloneqq \boldsymbol{A} - \beta_1(w_a \boldsymbol{f}_A + w_{at} \boldsymbol{f}_{AT} + w_{vt} \boldsymbol{f}_{VT} + w_{pt} \boldsymbol{f}_{PT}) \tag{26k}$$

$$t_F \coloneqq t_F - \beta_2(w_{tf} + w_{at} f_{ATF} + w_{vt} f_{VTF} + w_{pt} f_{PTF}) \tag{26l}$$

$$\boldsymbol{V} \coloneqq \boldsymbol{D}_{3N} \boldsymbol{A} \tag{26m}$$

$$\boldsymbol{P} \coloneqq \boldsymbol{D}_{3N} \boldsymbol{V} \tag{26n}$$

$$\beta_1 \coloneqq \beta_1 - R\beta_{1,0} \tag{26o}$$

$$\text{if } \ q > 5 \wedge \forall x \in \{J_{AT,q}, J_{VT,q}, J_{PT,q}\}, \begin{cases} |x_{q-4} - x_{q-5}| < \varepsilon\, |x_{q-5}| \\ |x_{q-3} - x_{q-4}| < \varepsilon\, |x_{q-4}| \\ |x_{q-2} - x_{q-3}| < \varepsilon\, |x_{q-3}| \\ |x_{q-1} - x_{q-2}| < \varepsilon\, |x_{q-2}| \\ |x_q - x_{q-1}| < \varepsilon\, |x_{q-1}| \end{cases} \tag{26p}$$

$$\quad \text{then break} \tag{26q}$$

$$\text{end if} \tag{26r}$$

$$\text{end for} \tag{26s}$$

where $\boldsymbol{A}_0 \in \mathbb{R}^{3N}$ represents an initial trajectory, a trapezoidal acceleration trajectory created using the maximum acceleration and velocity of the specifications. $\varepsilon \in \mathbb{R}$ is the relative change rate between iterations. Using this, the

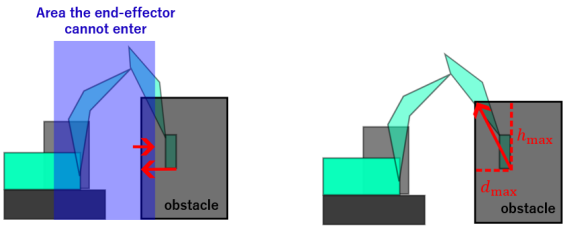

(a) The impenetrable area. (b) The diagonal penalty.

Fig. 3: Penalty for collision avoidance.

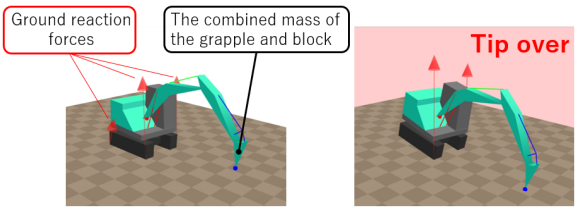

Fig. 4: Excavator in the simulation.

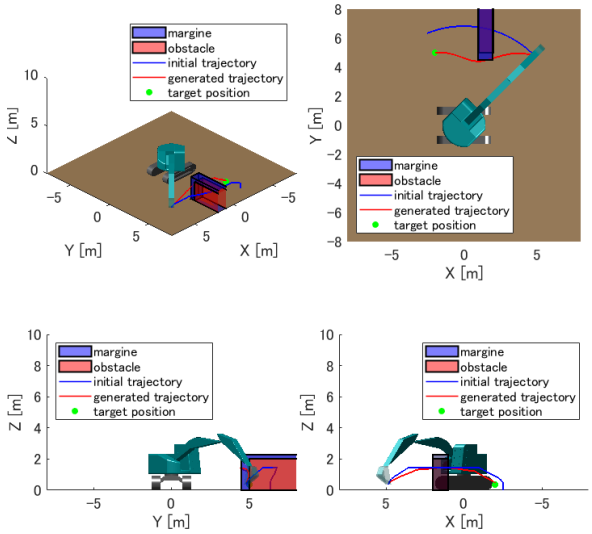

Fig. 5: Initial and generated trajectories.

iteration is terminated when the change in the value of the penalty function is very small for five consecutive iterations. The time-series data of the end-effector's position obtained by this algorithm are followed by an automatic excavator to prevent tipping over and collisions during tasks.

C. Penalty for Collision Avoidance

When the initial trajectory passes through an obstacle, a trajectory is generated to avoid it in the radial or vertical direction. However, suppose the avoidance direction is limited to one direction. In this case, the avoidance trajectory cannot be obtained if the end-effector attempts to enter the impenetrable area, as shown in Fig. 3(a). Therefore, the diagonal modification is performed once every n_{ite} iterations as shown in Fig. 3(b). This automatically generates a vertical avoidance trajectory even when a radial avoidance trajectory cannot be obtained, as shown in Fig. 3(a).

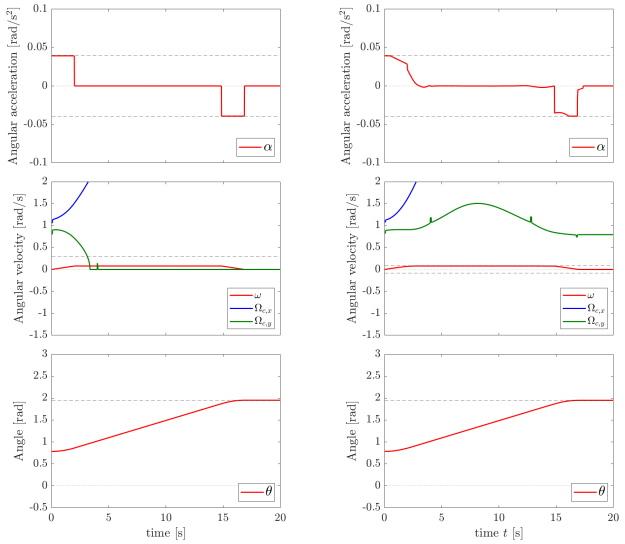

(a) θ coordinates: initial. (b) θ coordinates: generated.

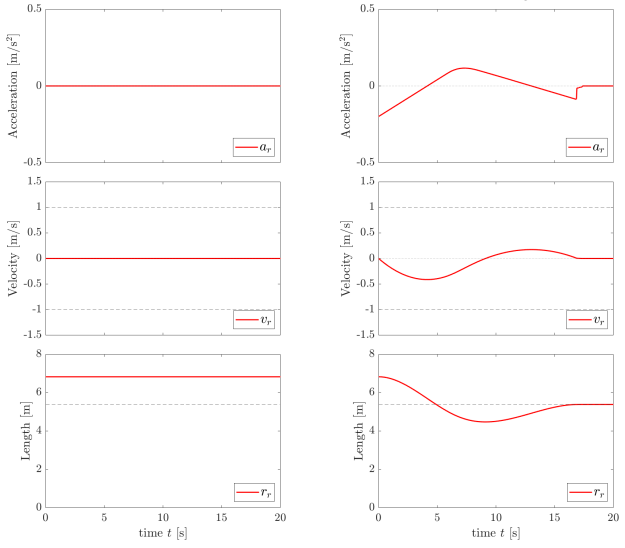

(c) r_r coordinates: initial. (d) r_r coordinates: generated.

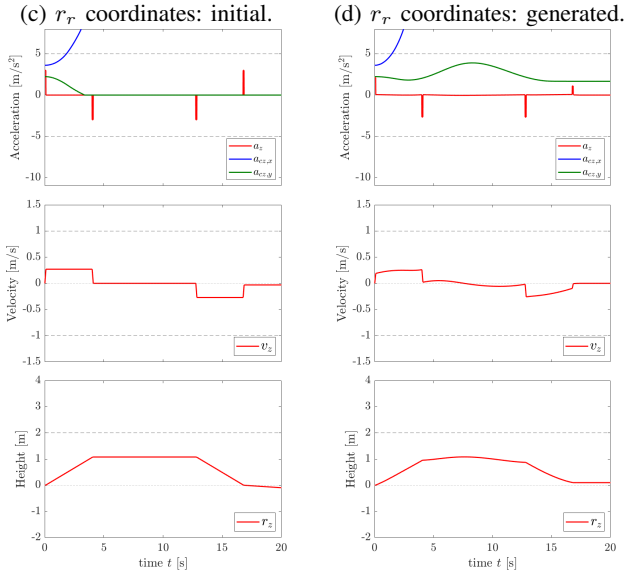

(e) r_z coordinates: initial. (f) r_z coordinates: generated.

Fig. 6: Initial and generated trajectories.

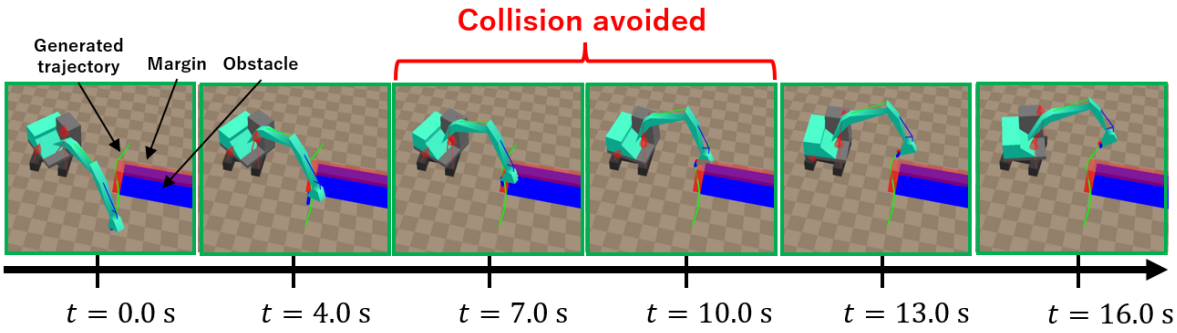

Fig. 7: Simulation result about following the trajectory.

IV. Simulations

A. Simulator Setting

The effectiveness of the generated trajectory was verified by using a simulator for a 13-ton class hydraulic excavator. The simulation environment was developed by Murata et al [4]. It is based on a nonsmooth quasi-static hydraulic model of Kikuuwe et al [5]. Each link is a rigid body with six degrees of freedom in the simulator, and the joints are represented as virtual spring-dampers. The excavator in the simulator was controlled by the position controller developed by Yamamoto et al. [6].

Fig. 4 shows the excavator during the simulation. The mass of the end-effector link of the excavator is set to the combined mass of the grapple and block, simulating the condition where the excavator is gripping the block. Additionally, the mass of the block is set at approximately two times the actual value, assuming a situation where the excavator is likely to tip over. Tipping over occurs when the ground reaction force at two of the four corners of the support polygon becomes 0 kN. When tipping over is detected, the background color of the simulation changes to red. The parameters for the specifications of the excavator were $\alpha_{\mathrm{sp}} = 0.04$ rad/s, $\omega_{\mathrm{sp}} = 0.08$ rad/s, $a_{z,\mathrm{sp}} = 3.00$ m/s, $v_{z,\mathrm{sp}} = 0.25$ m/s, $a_{r,\mathrm{sp}} = 5.00$ m/s, $v_{r,\mathrm{sp}} = 1.0$ m/s, $r_{r,\mathrm{sp,max}} = 5.50$ m, $r_{r,\mathrm{sp,min}} = 4.20$ m, and $h_l = 0.50$ m. In addition, the parameters for the iteration in the algorithm are $w_a = 0.10$, $w_{tf} = 0.001$ m^2/s^5, $w_{at} = 15.0$ m/s^2, $w_{vt} = 15.0$ m/s^3, $w_{pt} = 4.00$ m/s^4, $\beta_{1,0} = 0.0008$, $\beta_2 = 0.0001$, $N = 3000$, $Q = 5000$, $R = 1/5000$, and $n_{ite} = 5$.

B. Simulation Result

A trajectory was generated for carrying a block placed in the left front of an excavator to the left rear. In this task, an obstacle is placed on the line connecting the initial and target points. The generated trajectory is shown in Fig. 5 and Fig. 6. In Fig. 5, the initial trajectory was a simple one created based on the parameters of the specifications. The generated trajectory was an appropriate one satisfying the constraints. From this, it is confirmed that the generated trajectory avoids obstacles. In Fig. 6, while some parts of the initial trajectory exceed the tipping-over limits, it can be seen that the generated one does not exceed these limits. From this, it is confirmed that the trajectory that prevents tipping over has been generated.

The automatic excavator followed the generated trajectory in the simulation. Fig. 7 shows how the excavator tracked the trajectory, with the green curve representing the generated trajectory. The excavator successfully completed the task without its body lifting off the ground. This indicates that the proposed method avoided collisions with obstacles and prevented the excavator from tipping over.

V. Conclusion

This paper has proposed a method for generating end-effector trajectories for automatic hydraulic excavators. The method enables the automatic generation of trajectories that allow for efficient task completion while preventing tipping over and avoiding collisions with obstacles. The generated trajectory was followed by the excavator in simulations, and it was confirmed that no tipping over and no collisions occurred. While the effectiveness of the proposed method was confirmed in simulations, several issues remain. For example, obstacle avoidance is not yet possible in cases where obstacles are located in various directions around the excavator. Furthermore, implementing a user interface that allows non-expert operators to generate trajectories intuitively is also essential for practical deployment.

References

[1] R. Tsuzuki, K. Hara, and D. Usui, “Development of a highly efficient trajectory planning algorithm in backfilling task for autonomous excavators by imitation of experts and numerical optimization,” *Journal of Robotics and Mechatronics*, Vol.36 No.2, pp. 263-272, 2024.

[2] B. Son, C. Kim, C. Kim and D. Lee, ”Expert-emulating excavation trajectory planning for autonomous robotic industrial excavator,” in *Proceedings of the 2020 IEEE/RSJ International Conference on Intelligent Robots and Systems (IROS)*, 2020, pp. 2656-2662.

[3] Y. Zhang, Z. Sun, Q. Sun, Y. Wang, X. Li and J. Yang, ”Time-jerk optimal trajectory planning of hydraulic robotic excavator.” *Advances in Mechanical Engineering*, Vol.13, No.7, pp. 1-13, 2021.

[4] K. Murata, R. Kikuuwe, T. Okada, H. Yoshihara, T. Doi, T. Nanjo, and K. Yamashita, “Realtime simulation techniques for hydraulic excavators,” in *Proceedings of the 20th SICE System Integration Division Annual Conference*, 2019, pp. 2526–2531, (in Japanese).

[5] R. Kikuuwe, T. Okada, H. Yoshihara, T. Doi, T. Nanjo, and K. Yamashita, “A nonsmooth quasi-static modeling approach for hydraulic actuators,” *ASME Journal of Dynamic Systems, Measurement, and Control*, vol. 143, no. 12, p. 121002, 2021.

[6] Y. Yamamoto, J. Qiu, T. Doi, T. Nanjo, K. Yamashita and R. Kikuuwe, ”A position controller for hydraulic excavators with deadtime and regenerative pipelines,” *IEEE Transactions on Automation Science and Engineering*, vol. 22, pp. 855-871, 2025.